Astron. Astrophys. 361, 629–640 (2000)

ASTRONOMY AND ASTROPHYSICS

The nature of the DAB white dwarf HS 0209+0832⋆

B. Wolff[1], **S. Jordan**[1], **D. Koester**[1], **and D. Reimers**[2]

[1] Institut für Theoretische Physik und Astrophysik, Universität Kiel, 24098 Kiel, Germany (wolff,jordan,koester@astrophysik.uni-kiel.de)
[2] Hamburger Sternwarte, Universität Hamburg, Gojenbergsweg 112, 21029 Hamburg, Germany

Received 17 April 2000 / Accepted 11 July 2000

Abstract. The DAB white dwarf HS 0209+0832 is one of the few white dwarfs with detected helium in the DB gap between 28 000 and 45 000 K. We have obtained ultraviolet and optical spectra with the Hubble Space Telescope (HST). The analysis results in an effective temperature of about 35 000 K and a helium abundance of about 1%. The presence of C IV at 1548 Å, which was earlier detected by the International Ultraviolet Explorer (IUE), is confirmed. Additionally, we could identify more than 140 photospheric and 12 interstellar metal lines. For the first time we have found aluminum, calcium, titanium, nickel, and zinc, which cannot be supported by radiative levitation at such a low effective temperature. With stratified model atmospheres we tested, whether HS 0209+0832 has a very thin layer of hydrogen ($\approx 10^{-16}\,M_\odot$) on top of the helium envelope so that it is not thick enough to hide all the helium as is usually assumed to explain the DB gap. From the detailed shape of the He II 1640 Å line we could exclude such a model and conclude that diffusion equilibrium has not yet been reached; all observations are compatible with almost homogeneously mixed atmospheres, as would also be expected from the presence of metal lines. The most probable explanation is that HS 0209+0832 is still accreting matter from an interstellar cloud and that helium and metals would sink downwards, if no longer supplied from the surrounding medium. The finding by Heber et al. (1997) that the He I line at 4471 Å has been weaker by a factor of two or three for several months would fit into this scenario, if we assume that HS 0209+0832 travels through an inhomogeneous medium.

Key words: stars: abundances – stars: atmospheres – stars: individual: HS 0209+0832 – stars: white dwarfs – ultraviolet: stars

1. Introduction

The chemical composition of white dwarfs is rather peculiar. Normally, only the lightest element shows up in optical spectra. The reason for this almost mono-elemental composition has been known for a long time. Schatzman (1949, 1958) has shown that the huge gravitational acceleration leads to downward diffusion of heavier elements, which is fast compared to the evolutionary time scale.

Whether the atmosphere of a white dwarf is hydrogen-rich (spectral type DA) or helium-rich (non-DA: DB, DO) at the hot end of the cooling sequence is probably decided by the pre-white dwarf evolution, particularly by the exact phase, when the star leaves the AGB. According to evolutionary calculations $10^{-4}\,M_\odot$ of hydrogen is left over when nuclear burning finally ceases in the hydrogen shell. However, a late thermal pulse in a post-AGB star may lead to an almost complete loss of hydrogen and therefore to a non-DA atmosphere (Iben & McDonald 1995, Herwig et al. 1999).

It is clear that not all white dwarfs remain in their spectral class during the whole cooling time. Particularly, between 28 000 K and 45 000 K not a single non-DA star is known (Liebert et al. 1986). Up to now, no comprehensive explanation has been found for this DB gap. The most popular explanation is that small amounts of hydrogen are hidden in the atmosphere of a DO white dwarf, which float up until the star has cooled down to about 45 000 K. A hydrogen layer of $10^{-14}\,M_\odot$ on top of the helium envelope is sufficient to let the white dwarf look like a DA. At $T_{\rm eff} \approx 28\,000$ K the convection zone of He II begins to reach into the photosphere so that hydrogen and helium are mixed completely. The white dwarf develops again a helium-rich atmosphere (Fontaine & Wesemael 1987).

In order to provide further constraints for an understanding of the atmospheric composition of white dwarfs, the very few objects with hybrid atmospheres consisting of both lightest elements are of great importance. Among these, HS 0209+0832 is particularly interesting because it is besides GD 50 (Vennes et al. 1996) the only white dwarf between 28 000 and 45 000 K where helium ($\approx$ 1–2%) could be detected in the otherwise hydrogen rich atmosphere (Jordan et al. 1993). At the temperature of HS 0209+0832 ($T_{\rm eff} \approx 35\,000$ K), helium is expected to diffuse out of the hydrogen atmosphere on a time scale of only a few months (see e.g. Vennes et al. 1988, Koester 1989). Physical processes must exist preventing helium from settling down or helium must be supplied continuously, e.g. by accretion.

HS 0209+0832 became even more interesting, when Heber et al. (1997) found that the strength of the He I line at 4471 Å may not be constant. In one spectrum helium was reduced by

Send offprint requests to: B. Wolff

⋆ Based on observations made with the NASA/ESA Hubble Space Telescope, obtained at the Space Telescope Science Institute, which is operated by the Association of Universities for Research in Astronomy, Inc., under NASA contract NAS 5-26555. These observations are associated with proposal ID 7473.

Table 1. HST/STIS observations from January 10, 1999

Detector	Time / sec	Grating	λ/ Å	$\lambda/2\Delta\lambda$
MAMA	2110	E140M	1150–1700	45800
MAMA	1140	E140M	1150–1700	45800
CCD	600	G230LB	1685–3065	615–1135
CCD	320	G430L	2900–5700	530–1040

a factor of 2–3 relative to the other observations. Eight months later the previous helium abundance was measured again. A variable helium line at 4471 Å has also been reported for the DAB G 104-27 with an effective temperature just below the DB gap. While Holberg et al. (1990) detected helium, neither Kidder et al. (1992) nor Finley et al. (1997) confirmed its presence.

Besides helium, C IV could also be observed in the atmosphere of HS 0209+0832 with a spectrum of low signal-to-noise taken with the IUE satellite (Jordan et al. 1993). As in the case of helium, carbon cannot be supported by radiative acceleration in the atmosphere. According to the calculations of Chayer et al. (1995) only $\mathrm{C/H} \approx 6 \cdot 10^{-8}$ can be explained by radiative levitation – compared to $\approx 10^{-4}$ as determined by Jordan et al. (1993).

The aim of our HST observation of HS 0209+0832 was to look for He II 1640 Å, to confirm the detection of carbon, to search for additional metals, and to precisely determine the effective temperature from the energy distribution and the shape of the hydrogen lines. Unfortunately, the observation was delayed for more than a year due to the problems with the NICMOS detector and the resulting preference for infrared observations.

In this paper we present an analysis of the HST spectra. Sect. 2 contains a description of the observations. These are analyzed in Sect. 3 and in Sect. 4 with different assumptions for the atmospheric structure. In Sect. 5, we discuss possible explanations for HS 0209+0832 and conclude with a general discussion in Sect. 6.

2. Observations

HS 0209+0832 was observed on January 10, 1999 with the Space Telescope Imaging Spectrograph (STIS) onboard HST. Four exposures in three different wavelengths regions have been carried out during two orbits. The spectra cover the entire range from 1150 Å to 5700 Å with a resolution of ≈ 0.03 Å in the far ultraviolet and ≈ 5 Å in the optical. Table 1 contains an overview of the observations. The data were reduced with the standard procedures of the STSDAS package in IRAF using the latest available reference files (February 2000).

The observed spectral range contains the hydrogen Balmer lines (Hβ and higher) which can be used to determine effective temperature and gravity. The continuum slope from the optical to the ultraviolet and Lα can serve as additional temperature indicators. The helium abundance can be determined from the He I line at 4471 Å and the He II line at 1640 Å.

At the time of the planning of the HST observation it was not known that HS 0209+0832 may have variable helium features. Therefore, the exposures were only taken on a single date and were not prepared to search for variability. The E140M (FUV) observation is, however, splitted into two exposures but the He II line at 1640 Å does not vary in strengths between these exposures. The gap between the exposures was 47 minutes which is much shorter than the time scale of eight months by which the line strength varied according to Heber et al. (1997).

We have also compared the new optical observations of the He I line at 4471 Å with the observations from 1990 but did not find significant variations. Note, however, that both observations have only medium resolution (7 Å and 5 Å) and medium signal-to-noise ($\mathrm{S/N} \approx 30$). For the HST observations, the main focus of the optical spectrum aimed at a precise determination of the overall energy distribution.

The FUV spectra contain besides Lα and He II 1640 Å about 250 interstellar and photospheric lines. In particular, interstellar features from C II, N I, O I, Si II, and S I as well as stellar lines from C III, C IV, Al III, Si III, Si IV, Ca III, Ti III, Ti IV, Ni III, Ni IV, Zn III, and Zn IV can be identified.

3. Analysis with homogeneous atmospheres

3.1. Hydrogen and helium lines

The simplest approach is the assumption of a homogeneous distribution of hydrogen and helium. We use line-blanketed LTE model atmospheres; the absorption of helium and metals in the extreme ultraviolet is completely taken into account. A recent description of the procedures for the calculation of theoretical atmospheres and synthetic spectra is given by Finley et al. (1997).

We started by assuming $T_{\rm eff} = 36\,000$ K and $\log g = 8.0$ and determined an approximate helium abundance from the lines at 1640 Å and 4471 Å by a visual comparison of synthetic spectra and observations. Subsequently, $T_{\rm eff}$ and $\log g$ were calculated from the hydrogen Balmer line profiles using a χ^2 method. The result is $T_{\rm eff} = 35\,500 \pm 200$ K and $\log g = 7.90 \pm 0.04$.

The He I line at 4471 Å can be reproduced best with $\mathrm{He/H} = (1.1 \pm 0.4) \cdot 10^{-2}$ (Fig. 1). This abundance is somewhat too low for the He II line at 1640 Å which can be fitted better with $\mathrm{He/H} = 3.0 \cdot 10^{-2}$ (Fig. 2). The discrepancy between these lines can be removed if $T_{\rm eff}$ is increased to about 40 000 K. Then, both lines can be fitted with $\mathrm{He/H} = 1.5 \cdot 10^{-2}$, but the temperature required is out of the error range from the Balmer line analysis. The different helium abundances do not influence the determination of $T_{\rm eff}$ and $\log g$ from the Balmer lines.

The continuum slope and the Lα line can be used as additional temperature constraints. However, both the E140M and G230LB spectra suffer from uncertainties in the flux calibration. The flux in the Lα core reaches negative values because the scattered light in the echelle modes of STIS cannot be removed correctly with the currently available calibration software. For the G230LB grating there are problems with the throughput correction for the aperture used ($52'' \times 0.5''$). This can be seen in the overlap region of the E140M and G230LB spectra where the G230LB flux is lower than the E140M flux. Nevertheless, the

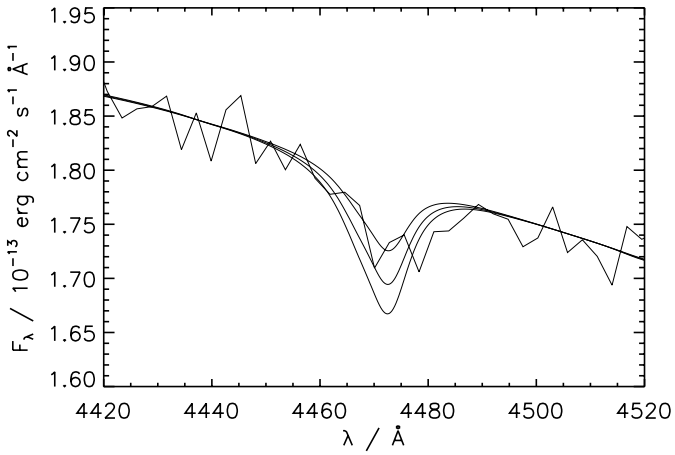

Fig. 1. He I line compared to homogeneous hydrogen-helium models with $T_{\rm eff} = 35\,500$ K, $\log g = 7.9$, and $\mathrm{He/H} = 0.7, 1.1, 1.5$ % (from top to bottom)

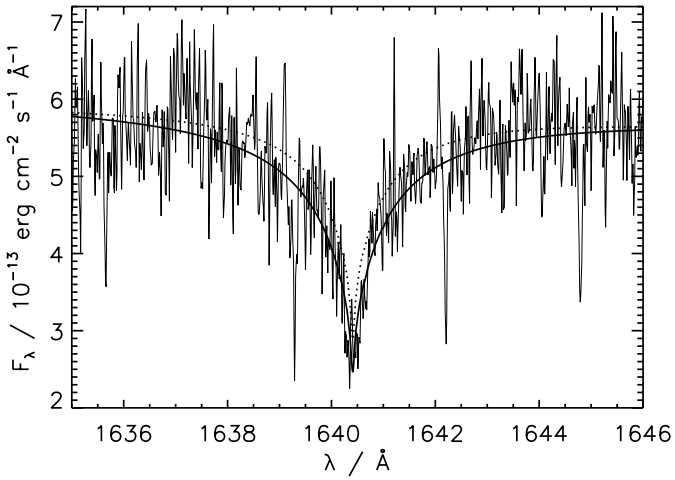

Fig. 2. He II line compared to homogeneous hydrogen-helium models with $T_{\rm eff} = 35\,500$ K, $\log g = 7.9$, and $\mathrm{He/H} = 1.1$ % (dotted line) and 3.0 % (full line). The observed spectrum is corrected for the radial velocity of HS 0209+0832 (see Sect. 3.2)

model for $T_{\rm eff} = 35\,500$ K can reproduce the continuum slope in the optical and near ultraviolet ($\lambda > 2500$ K) if we fit the model to the G430L spectrum at 5500 Å (see Fig. 3). From the shape of the Lα line (with the exception of the core and regions with metal lines) $T_{\rm eff} = 35\,900 \pm 300$ K and $\log g = 7.79 \pm 0.06$ can be derived (see Fig. 4).

Our temperature and gravity determinations are consistent with the results of Jordan et al. (1993, $T_{\rm eff} = 36\,000 \pm 2000$ K) and Heber et al. (1997, $T_{\rm eff} = 36\,100 \pm 200$ K, $\log g = 7.91 \pm 0.05$). The latter analysis is the mean of five individual measurements varying by about 500 K so that our single measurement is compatible although the formal errors of the mean results do not overlap.

The new helium abundance is at the high end of the observed range: The analyses of both the 1990 and 1996 observations by Heber et al. give a mean value of $1.16 \cdot 10^{-2}$ whereas only the 1995 observation gives $0.47 \cdot 10^{-2}$ (Table 2). We have re-

Table 2. Helium abundance determinations for HS 0209+0832

Obs. date	He/H	Reference
10/08/90 10/09/90	$1.30 \cdot 10^{-2}$	this paper
10/08/90	$1.32 \cdot 10^{-2}$	Heber et al.
10/09/90	$1.00 \cdot 10^{-2}$	Heber et al.
12/23/95	$0.47 \cdot 10^{-2}$	Heber et al.
08/17/96	$1.20 \cdot 10^{-2}$	Heber et al.
08/18/96	$1.12 \cdot 10^{-2}$	Heber et al.
01/10/99	$1.10 \cdot 10^{-2}$	this paper

analyzed the 1990 observations with new model atmospheres resulting in $\mathrm{He/H} = 1.3 \cdot 10^{-2}$. The new observations are clearly at variance with an abundance as low as $0.5 \cdot 10^{-2}$.

Heber et al. analyzed all optical helium lines together and did not derive a seperate helium abundance for He II 4686 Å. From their fits it is not excluded that He II in the 1996 observations requires also a higher abundance but the line may be too shallow for a clear determination. In the next section the problem of the helium abundance is discussed together with the abundances of heavier elements.

3.2. Metal lines

The FUV spectrum of HS 0209+0832 exhibits about 250 lines from metals. We have determined their central wavelengths using a gaussian fit routine and have tried to identify all lines with the help of the lists from the Kurucz CD-ROM No. 23 (Kurucz & Bell 1995). Two systems with different apparent Doppler velocities can be distinguished. There are several resonance lines from C II, N I, O I and Si II with a mean Doppler velocity of $6.09 \pm 1.57\ \mathrm{km\,s^{-1}}$ (1σ). These lines are most probably interstellar because these low ionization stages cannot exist in an atmosphere as hot as $T_{\rm eff} = 35\,500$ K. The other system has an apparent velocity of $81.99 \pm 4.68\ \mathrm{km\,s^{-1}}$. Since it contains several higher ionized lines with non-zero excitation energy (e.g. C III at 1175 Å) we believe that all lines with this velocity are of photospheric origin. This system comprises lines of C III, C IV, Si III, Si IV, Al III, Ca III, Ti III, Ti IV, Ni III, Ni IV, Zn III, and Zn IV. The identified interstellar and the most prominent photospheric lines (E.W. $\gtrsim 10$ mÅ) are listed in Tables 3 and 4.

The composition of the atmosphere is rather unusual. Whereas carbon and silicon are also detected in several hot DA white dwarfs (e.g. Bruhweiler & Kondo 1981, Dupree & Raymond 1982, and later observations), calcium, titanium, nickel, and zinc have been identified for the first time in a white dwarf with $T_{\rm eff} \approx 35\,000$ K. Therefore, we have tested whether lines from different elements belong to systems with slightly different velocities. This is not the case: The apparent velocity is $81.48 \pm 1.64\ \mathrm{km\,s^{-1}}$ for the carbon and silicon lines together, $84.04 \pm 1.99\ \mathrm{km\,s^{-1}}$ for calcium, $82.13 \pm 5.10\ \mathrm{km\,s^{-1}}$ for titanium, $82.55 \pm 4.43\ \mathrm{km\,s^{-1}}$ for nickel, and $81.63 \pm 5.26\ \mathrm{km\,s^{-1}}$

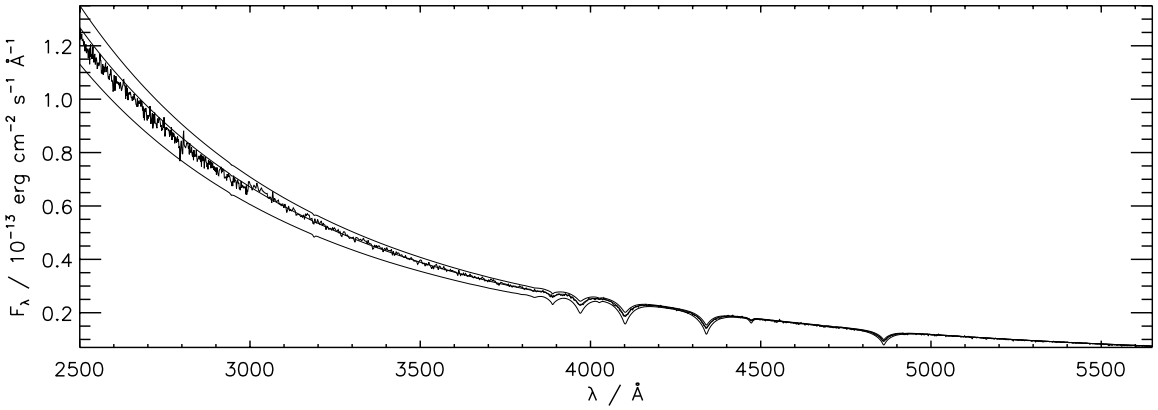

Fig. 3. Optical and near ultraviolet spectrum compared to models with $T_{\rm eff} = 31,000$ K, 35 500 K, and 40 000 K. All models have $\log g = 7.9$ and $\rm He/H = 1.1\,\%$

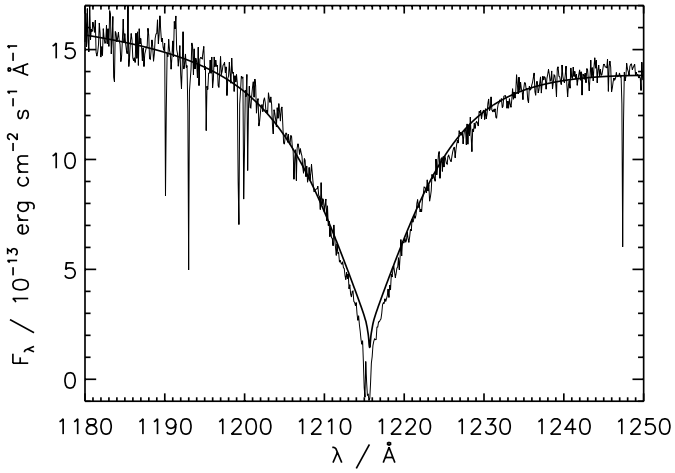

Fig. 4. Lα line compared to a model with $T_{\rm eff} = 35\,900$ K and $\log g = 7.79$. The observed spectrum is rebinned to a resolution of 0.1 Å for clarity.

Table 3. Interstellar lines

Ion	λ/Å (lab.)	λ/Å (obs.)	E.W./mÅ	$V/\mathrm{km\,s^{-1}}$
Si II	1190.416	1190.437	70.3	5.29
Si II	1193.290	1193.312	94.6	5.52
N I	1199.550	1199.579	78.6	7.23
N I	1200.223	1200.252	63.0	7.23
N I	1200.710	1200.745	41.6	8.75
S II	1259.519	1259.534	18.4	3.57
Si II	1260.422	1260.446	116.3	5.72
S I	1295.653	1295.684	16.0	7.17
O I	1302.168	1302.201	126.4	7.62
Si II	1304.370	1304.388	41.0	4.12
C II	1334.532	1334.560	165.9	6.31
Si II	1526.707	1526.730	62.9	4.51
				$< V >= 6.09$

for zinc. Since these velocities are very similar a common origin of all lines seems to be plausible.

Table 5 contains a list of abundances derived from comparisons with model atmospheres. Upper limits for several elements are also given. In Figs. 5, 6, and 7 we show example fits of several photospheric lines. For the two ionization stages of zinc oscillator strengths are only available for Zn III. The wavelengths of the Zn IV lines with the largest intensities observed in laboratory spectra have been taken from Sugar & Musgrove (1995) and Crooker & Dick (1968). The inferred velocity for these lines is $80.44 \pm 4.50\,\mathrm{km\,s^{-1}}$, in agreement with the velociy of the Zn III lines ($82.59 \pm 5.80\,\mathrm{km\,s^{-1}}$).

Before the HST observations were obtained only the C IV lines at 1548.187 Å and 1550.772 Å could be identified with IUE. Jordan et al. (1993) derived $\rm C/H = 1 \cdot 10^{-4}$ – more than one order of magnitude higher than our determination from the STIS spectra. A direct comparison of the IUE and STIS observations shows that the C IV lines in the IUE spectrum are indeed much stronger. However, we cannot be sure that the variation is real due to the low signal-to-noise ratio of the IUE observation.

The carbon and titanium abundances need some discussion, because the fit to different ionization stages gives different results. From the C III lines we derive $\rm C/H = 1.25 \cdot 10^{-6}$ whereas C IV gives $\rm C/H = 7.5 \cdot 10^{-6}$. The situation for titanium is similar: $\rm Ti/H = 3 \cdot 10^{-7}$ from Ti III and $\rm Ti/H = 1 \cdot 10^{-6}$ from Ti IV. These discrepancies can be removed if the effective temperature is increased to 40 000 K. Then, the abundances are $\rm C/H = 2.5 \cdot 10^{-6}$ and $\rm Ti/H = 1 \cdot 10^{-6}$. This is the same problem as with He I and He II. An effective temperature of $\approx$ 40 000 K is clearly ruled out by the Balmer lines, Lα, and the optical slope.

The discrepant abundance determinations are typical non-LTE effects. This may be the best explanation although the effective temperature of HS 0209+0832 is rather low. We have included the uncertainties from the choice of the ionization stage for the errors given in Table 5 for the abundances.

The large amount of heavy elements could also affect the flux distribution and therefore the determination of $T_{\rm eff}$ due to the line blanketing and backwarming effects. We have included the EUV opacities of the metals in the model calculations. However, most of the EUV flux is already absorbed by helium so that

Table 4. Photospheric lines

Ion	λ/Å (lab.)	λ/Å (obs.)	E.W./mÅ	$V/\mathrm{km\,s^{-1}}$	Ion	λ/Å (lab.)	λ/Å (obs.)	E.W./mÅ	$V/\mathrm{km\,s^{-1}}$
C III	1174.933	1175.250	113.7	80.89	Zn IV	1340.16	1340.452	17.7	65.32
C III	1175.263	1175.582	109.6	81.40	Zn IV	1342.72	1343.113	15.5	87.74
C III	1175.590	1175.901	86.3	79.32	Zn III	1343.346	1343.745	13.5	89.04
C III	1175.711	1176.027	124.4	80.55	Zn IV	1343.79	1344.177	20.3	86.34
C III	1175.987	1176.308	98.9	81.81	Zn IV	1344.08	1344.449	24.9	82.30
C III	1176.370	1176.685	113.2	80.29	Zn IV	1347.98	1348.329	18.4	77.62
Ti IV	1195.204	1195.542	24.9	84.78	Zn IV	1349.90	1350.255	24.3	78.84
Si III	1206.500	1206.826	17.4	81.02	Zn IV	1352.88	1353.262	42.6	84.65
C III	1247.370	1247.728	79.0	86.05	Ni IV	1357.064	1357.440	14.8	83.06
Zn III	1253.299	1253.686	10.8	92.57	Zn IV	1357.82	1358.182	21.8	79.93
Zn III	1262.508	1262.894	21.2	91.66	Zn IV	1359.46	1359.856	14.6	87.33
Zn IV	1265.74	1266.070	29.2	78.16	Zn III	1359.601	1359.998	9.8	87.54
Ca III	1278.393	1278.745	11.2	82.56	Zn III	1359.799	1360.197	16.7	87.75
Zn IV	1272.21	1272.538	15.2	77.29	Zn III	1362.520	1362.919	17.9	87.79
Zn IV	1272.98	1273.319	23.0	79.84	Zn IV	1363.43	1363.802	27.0	81.80
Zn III	1274.384	1274.756	10.6	87.51	Zn IV	1363.95	1364.294	31.6	75.61
Zn IV	1277.11	1277.485	24.0	88.03	Zn III	1364.323	1364.711	9.8	85.26
Zn IV	1280.47	1280.816	17.0	81.01	Zn IV	1365.23	1365.612	24.3	83.88
Zn IV	1283.50	1283.875	16.0	87.60	Zn III	1365.706	1366.093	21.0	84.95
Zn IV	1284.72	1285.085	16.5	85.17	Zn III	1366.968	1367.337	20.4	80.93
Ti III	1286.369	1286.726	34.3	83.18	Zn IV	1369.53	1369.880	28.4	76.61
Ca III	1286.525	1286.878	16.3	82.26	Zn III	1373.691	1374.101	22.7	89.48
Ti III	1289.299	1289.652	17.0	82.12	Zn IV	1375.33	1375.690	23.9	78.47
Ti III	1291.625	1291.975	24.6	81.24	Zn IV	1377.65	1378.004	28.7	77.03
Zn IV	1291.83	1292.158	20.3	76.12	Al III	1379.670	1380.038	12.1	79.95
Zn III	1292.212	1292.589	38.3	87.46	Zn IV	1387.22	1387.591	12.0	80.18
Zn IV	1292.49	1292.839	17.0	80.95	Zn IV	1387.70	1388.093	21.2	84.90
Ti III	1293.225	1293.575	19.8	81.13	Ni III	1393.042	1393.442	12.3	86.08
Ti III	1294.674	1295.050	33.2	87.09	Si IV	1393.755	1394.133	49.8	81.32
Ti III	1294.717	1295.050	31.7	77.11	Zn III	1394.910	1395.308	9.3	85.54
Ti III	1295.884	1296.235	20.9	81.19	Ni III	1396.118	1396.494	4.8	80.74
Zn IV	1296.62	1296.965	15.6	79.77	Ni IV	1398.193	1398.587	19.6	84.49
Zn IV	1296.73	1297.071	26.1	78.84	Ni IV	1399.947	1400.317	11.7	79.23
Ca III	1298.034	1298.400	20.9	84.52	Si IV	1402.770	1403.150	37.2	81.21
Ti III	1298.697	1299.022	62.4	75.01	Ni IV	1411.451	1411.845	16.1	83.67
Ti III	1298.996	1299.356	30.5	83.08	Ni IV	1414.597	1414.958	7.9	76.50
Zn IV	1301.20	1301.562	20.8	83.40	Ti III	1420.034	1420.393	25.8	75.77
Zn III	1303.535	1303.921	21.8	88.77	Ni IV	1421.216	1421.606	13.7	82.27
Zn IV	1306.66	1307.000	40.2	78.01	Ti III	1422.409	1422.787	22.3	79.65
Zn III	1307.350	1307.756	13.8	93.10	Ni IV	1430.190	1430.570	12.9	79.65
Ca III	1317.699	1318.061	6.0	82.37	Zn III	1432.148	1432.529	13.2	79.75
Zn IV	1318.00	1318.340	19.6	77.34	Ni IV	1438.814	1439.221	19.7	84.80
Zn III	1319.092	1319.488	30.4	90.00	Ni IV	1449.021	1449.404	13.0	79.25
Zn IV	1320.74	1321.081	29.1	77.40	Ti IV	1451.739	1452.145	30.4	83.84
Zn IV	1321.22	1321.563	28.6	77.83	Ni IV	1452.220	1452.612	6.4	80.94
Zn IV	1322.33	1322.682	26.1	79.80	Ca III	1453.161	1453.580	13.5	86.43
Zn IV	1322.43	1322.769	26.5	76.85	Ti III	1455.195	1455.573	34.3	77.88
Zn III	1323.501	1323.883	16.8	86.53	Zn III	1456.709	1457.104	30.0	81.29
Zn IV	1326.74	1327.092	18.0	79.54	Ca III	1459.793	1460.210	19.3	85.64
Ti III	1327.609	1327.973	20.1	82.20	Zn IV	1459.98	1460.353	25.0	76.59
Zn III	1328.367	1328.752	28.8	86.89	Ca III	1461.890	1462.300	5.6	84.09
Zn IV	1329.11	1329.469	23.9	80.97	Ca III	1463.341	1463.745	22.7	82.78
Zn IV	1329.92	1330.313	13.4	88.59	Zn III	1464.180	1464.589	27.0	83.74
Zn IV	1333.32	1333.676	19.0	80.04	Ti IV	1467.343	1467.748	41.5	82.75
Ca III	1335.128	1335.502	25.1	83.96	Ti IV	1469.191	1469.594	14.4	82.22

Table 4. (continued)

Ion	λ/Å (lab.)	λ/Å (obs.)	E.W./mÅ	$V/\mathrm{km\,s^{-1}}$
Zn III	1473.399	1473.799	51.4	81.39
Ca III	1484.868	1485.283	22.8	83.77
Zn III	1490.951	1491.336	24.6	77.41
Ca III	1496.883	1497.302	7.6	83.90
Zn III	1498.778	1499.107	25.5	65.81
Ti III	1498.695	1499.186	19.8	98.23
Zn III	1499.408	1499.817	41.3	81.78
Zn III	1500.411	1500.803	30.4	78.32
Zn III	1505.913	1506.310	30.0	79.03
Zn III	1515.834	1516.242	40.3	80.69
Ni IV	1534.710	1535.125	12.9	81.07
Ni IV	1543.372	1543.865	18.5	95.77
Ca III	1545.300	1545.731	38.4	83.60
C IV	1548.187	1548.613	132.9	82.50
C IV	1550.772	1551.193	115.0	81.39
Zn III	1552.284	1552.692	36.0	78.80
Zn III	1552.947	1553.346	27.1	77.03
Ca III	1555.526	1555.949	26.0	81.52
Zn III	1560.771	1561.203	38.2	82.98
Ca III	1562.464	1562.929	61.2	89.21
Zn III	1581.510	1581.923	53.2	78.29
Zn III	1582.036	1582.450	33.4	78.45
Zn III	1598.504	1598.935	30.1	80.83
Zn III	1600.863	1601.266	34.9	75.47
Al III	1611.873	1612.300	21.2	79.42
Zn III	1619.601	1620.034	34.2	80.15
Zn III	1622.505	1622.925	26.5	77.60
Zn III	1629.163	1629.600	52.7	80.41
Zn III	1639.320	1639.748	30.9	78.27
Zn III	1644.807	1645.250	36.3	80.74
Zn III	1651.738	1652.163	44.9	77.14
Zn III	1673.077	1673.471	62.5	70.60
Ni III	1692.508	1692.978	23.2	83.24
Ni III	1715.300	1715.758	26.1	80.05
				$< V >= 81.99$

Table 5. Photospheric abundances

Element	Abundance
He/H	$(1.1 \pm 0.4) \cdot 10^{-2}$
C/H	$(4.5 \pm 3.5) \cdot 10^{-6}$
N/H	$< 5.0 \cdot 10^{-6}$
O/H	$< 5.0 \cdot 10^{-5}$
Mg/H	$< 3.0 \cdot 10^{-4}$
Al/H	$(7.5 \pm 2.5) \cdot 10^{-8}$
Si/H	$(4.0 \pm 2.0) \cdot 10^{-9}$
Ca/H	$(2.0 \pm 1.0) \cdot 10^{-5}$
Ti/H	$(6.5 \pm 3.5) \cdot 10^{-7}$
Fe/H	$< 2.5 \cdot 10^{-7}$
Ni/H	$(5.0 \pm 3.0) \cdot 10^{-7}$
Zn/H	$(7.5 \pm 2.5) \cdot 10^{-8}$

metals are only of minor importance and, therefore, do not influence the temperature determination.

The abundance discrepancies could also be a hint that helium, carbon, and titanium are already diffused into deeper layers with somewhat higher temperature. In comparison to a homogeneous atmosphere the lines of these elements would be formed in larger depths where higher ionization stages are favored. This would support the assumption that helium and metals have been recently accreted onto HS 0209+0832 (see Sect. 5).

It is remarkable that iron lines could not be detected in the FUV spectrum, although nickel is identified. This is in contrast to all hotter DA white dwarfs, where more observations of iron lines exist than of nickel, and both elements have approximately the same abundances. However, the upper limit for the iron abundance is only a factor of two lower than the measured abundance for nickel so that a small amount of iron may be hidden. The reason for the lower abundance of iron is unclear.

About 100 lines remain unidentified (see Table 6). After identification of the most prominent interstellar and photospheric lines we have systematically calculated differences between the list of unidentified lines and lists extracted from the Kurucz CD-ROM. With this comparison we could identify several of the weaker lines. The search for additional metals is hampered by the lack of accurate oscillator strengths for atoms with high atmomic numbers. For instance, several lines could be identified with the strongest Cu IV lines from Meinders (1976) but other strong Cu IV lines are missing in the spectrum of HS 0209+0832. A clear decission would only be possible with reliable wavelengths, oscillator strengths, and calculations of model spectra.

We have also tested for molecular lines which are occasionally found in ultraviolet spectra of reddened stars. However, the usual features (Jenkis et al. 1973, van Dishoek & Black 1984) are not visible in the spectrum of HS 0209+0832.

4. Alternative models

In this section we discuss alternative models to explain the observed spectral features of HS 0209+0832.

Stratified atmosphere. The favored explanation for the DB gap predicts a small layer of hydrogen on top of a helium atmosphere for stars inside the gap. However, the presence of photospheric metals is in contradiction with this assumption, because it is difficult to understand why helium has settled down, whereas metals are still in the photosphere. Elements heavier than helium should sink down much faster. We have, nevertheless, tested whether HS 0209+0832 could have a stratified hydrogen-helium atmosphere, where the hydrogen layer is thin enough so that helium lines are still visible, in order to test the assumption of a homogeneously mixed atmosphere.

We have calculated stratified models with hydrogen and helium being in diffusion equilibrium. A general description of the physics and the computational methods has been given by Jordan & Koester (1986). Similar to the homogeneous case, we started with $T_{\mathrm{eff}} = 36\,000\,\mathrm{K}$ and $\log g = 8.0$, determined the

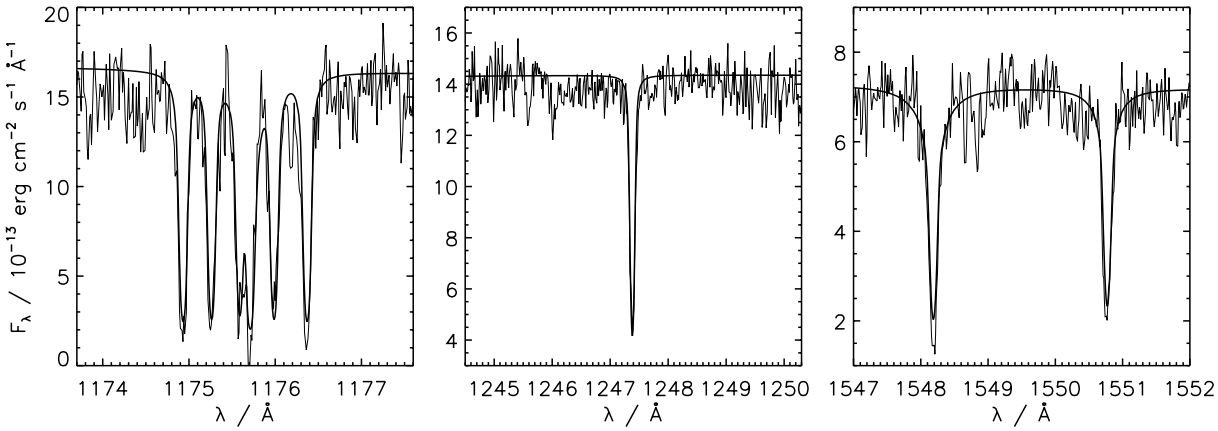

Fig. 5. Carbon lines: C III (left and middle) with $\mathrm{C/H} = 1.25 \cdot 10^{-6}$ and C IV (right) with $\mathrm{C/H} = 7.5 \cdot 10^{-6}$

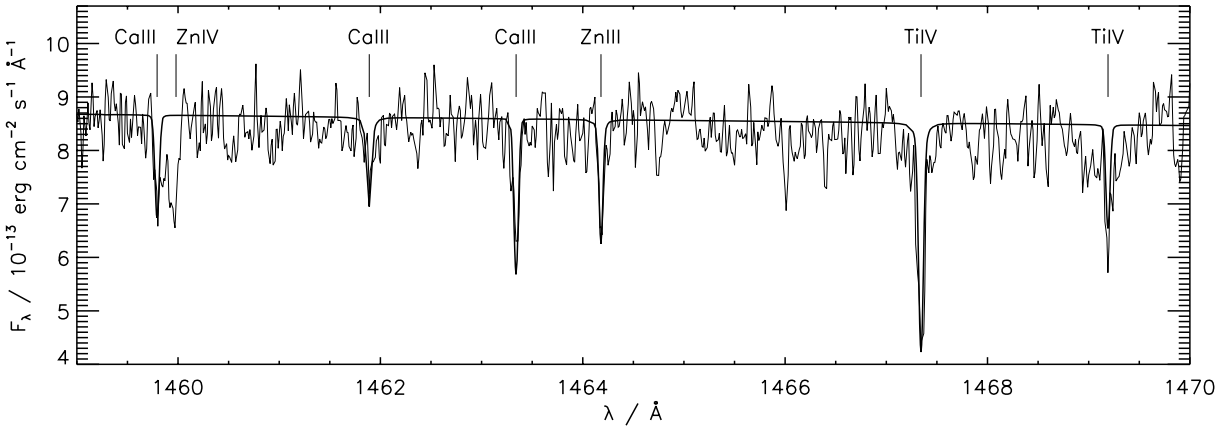

Fig. 6. Ca III ($\mathrm{Ca/H} = 2 \cdot 10^{-5}$), Ti IV ($\mathrm{Ti/H} = 1 \cdot 10^{-6}$), and Zn III ($\mathrm{Zn/H} = 7.5 \cdot 10^{-8}$) lines

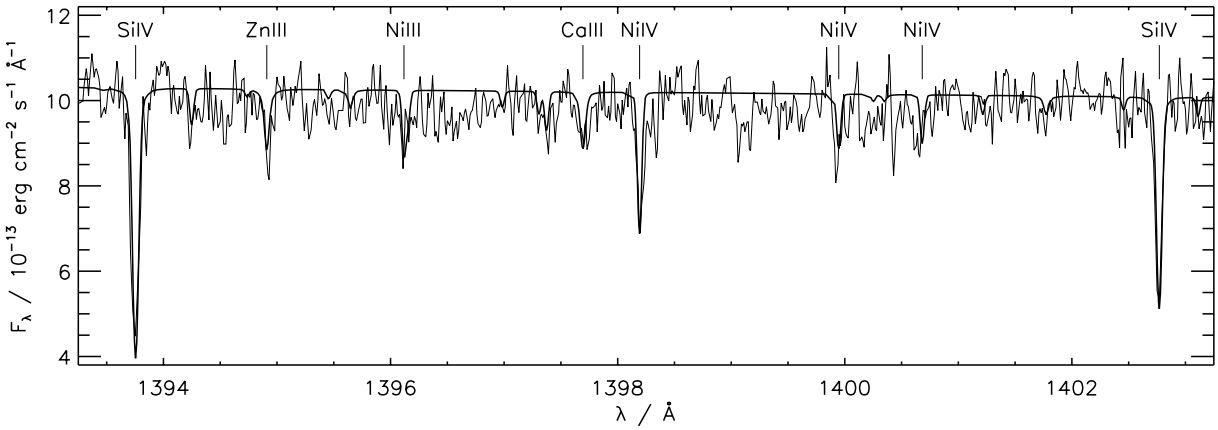

Fig. 7. Si IV ($\mathrm{Si/H} = 4 \cdot 10^{-9}$), Ca III ($\mathrm{Ca/H} = 2 \cdot 10^{-5}$), Ni III and Ni IV ($\mathrm{Ni/H} = 5 \cdot 10^{-7}$), and Zn III ($\mathrm{Zn/H} = 7.5 \cdot 10^{-8}$) lines

mass of the hydrogen layer from the strengths of the He I 4471 Å line, and used a χ^2 technique to calculate $T_{\rm eff}$ and $\log g$. It turned out that the shape of the He II 1640 Å line cannot be reproduced in detail and that the equivalent widths of the He II and He I line cannot be reproduced simultaneously. We have, therefore, used the optical line only. Two iterations were needed until the procedure converged with $T_{\rm eff} = 35\,000 \pm 200$ K, $\log g = 7.90 \pm 0.03$, and $M_{\rm H} = 1.5 \cdot 10^{-16}\,M_{\odot}$ for the mass of the hydrogen layer.

Fig. 8 shows the observed He II line at 1640 Å together with the stratified model, which can reproduce the optical He I line and the Balmer lines. The formal fit to the hydrogen lines is slightly worse than with homogeneous atmospheres ($\chi^2_{\rm r} = 1.82$ compared to $\chi^2_{\rm r} = 1.58$); the change of $\chi^2_{\rm r}$ is only small mainly due to the low signal-to-noise of the optical spectrum ($\mathrm{S/N} \approx 30$). However, the 1640 Å line of the stratified model is far too broad (Fig. 8) and the slope of the UV continuum

Table 6. Unidentified lines

λ/Å (obs.)	E.W./mÅ	λ/Å (obs.)	E.W./mÅ
1259.195	55.1	1446.703	14.4
1267.891	17.7	1447.887	25.7
1275.609	12.0	1450.065	15.6
1281.881	9.3	1466.411	8.9
1306.693	11.2	1472.623	5.4
1309.781	19.5	1473.055	27.5
1313.091	9.2	1477.373	42.8
1314.895	14.8	1487.638	10.2
1317.264	13.7	1500.972	28.6
1318.487	6.7	1502.698	24.8
1330.968	15.0	1509.131	22.0
1334.903	28.5	1509.499	7.7
1335.727	7.9	1511.248	31.3
1336.068	52.6	1514.241	14.5
1340.542	14.5	1517.757	15.8
1348.167	7.6	1517.870	21.6
1350.011	11.3	1518.627	6.6
1355.820	14.9	1524.766	25.7
1362.402	29.1	1525.331	14.6
1364.133	18.9	1533.021	17.8
1367.911	29.7	1533.386	43.3
1372.505	15.9	1534.466	15.8
1376.165	13.3	1534.691	11.8
1377.162	13.2	1594.185	26.9
1379.864	14.3	1600.590	13.9
1381.183	11.0	1603.534	36.3
1382.934	9.2	1603.974	9.6
1383.515	5.4	1606.388	20.4
1385.393	9.8	1607.168	23.1
1386.278	5.0	1613.509	13.1
1386.547	4.6	1616.540	22.5
1386.617	17.5	1617.019	9.9
1389.172	18.2	1624.530	11.9
1390.815	7.6	1626.575	16.1
1392.505	17.4	1626.840	11.6
1400.819	6.3	1628.554	11.3
1410.427	10.8	1628.726	21.3
1410.945	22.5	1636.104	20.6
1411.971	13.1	1640.872	26.1
1412.619	16.6	1642.656	42.9
1413.453	11.1	1681.927	26.6
1417.004	208.7	1687.563	46.3
1419.270	12.6	1696.007	12.1
1424.768	18.1	1725.264	18.8
1427.028	8.5		
1429.911	8.0		
1430.511	9.3		
1430.744	6.2		
1432.346	21.6		
1434.531	15.8		
1434.630	30.5		
1441.680	359.6		
1442.827	13.7		
1443.547	11.0		
1444.839	24.0		

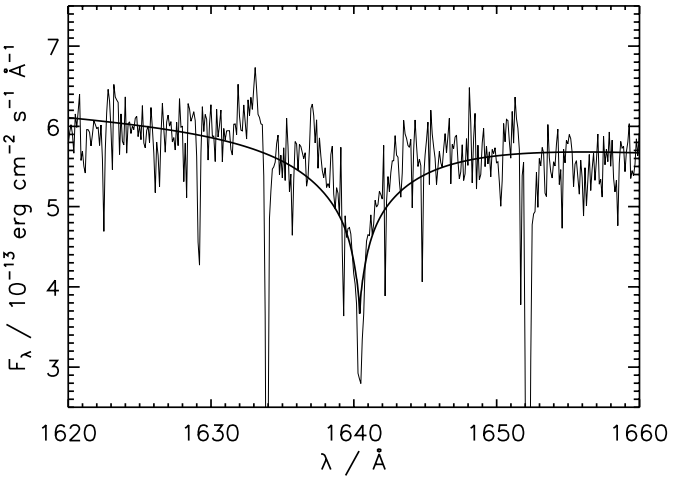

Fig. 8. He II line compared to a stratified hydrogen-helium model in diffusion equilibrium with $T_{\rm eff} = 35\,000$ K, $\log g = 7.9$, and $M_{\rm H} = 1.5 \cdot 10^{-16}\,M_\odot$. The observed spectrum is rebinned to a resolution of 0.1 Å for clarity. The gaps at 1634 Å and 1652 Å are gaps between the spectral orders

is also reproduced worse than in the homogeneously mixed case. Therefore, a stratified hydrogen-helium atmosphere in diffusion equilibrium is not able to explain the spectrum of HS 0209+0832. This confirms the conclusion of Jordan et al. (1993).

Non-uniform surface composition. Both models discussed so far assume that the elements are distributed uniformly over the surface of the star. A possibility to explain variable helium features as observed by Heber et al. (1997) is a slowly rotating star with a composition that varies over the surface. Such models have been applied with different success to several DAB white dwarfs (e.g. Achilleos et al. 1992, Kidder et al. 1992, Beauchamp et al. 1993, Koester et al. 1994). However, an inhomogeneous surface composition with extreme abundance variations – e.g. small helium spots in a pure hydrogen atmosphere – which has been discussed for some DABs is not suited to explain the spectrum of HS 0209+0832. This can be demonstrated with the strength of the UV He II line and the non-detection of the He I lines at 3187 Å and 2945 Å.

Let us consider first an equal temperature for the spots and the rest of the atmosphere. A pure DB model with $T_{\rm eff} = 35\,500$ K has already a He II 1640 Å line with about the same strengths as in the DAB model with $T_{\rm eff} = 35\,500$ K: The depths of the line is equal and only the wings are somewhat broader in the DB. Therefore, it is not possible to reproduce this line with a pure hydrogen atmosphere and additional helium spots of the same temperature. The pure helium region would have to contribute a significant amount of the total flux observed. This can only be achieved if it is hotter than the rest of the surface. This assumption is rather unlikely and cannot explain the whole spectrum either: If the equivalent width of the 1640 Å line is reproduced by a model, the He I lines at 3187 Å and 2945 Å would also be visible, unless the helium region is hotter than

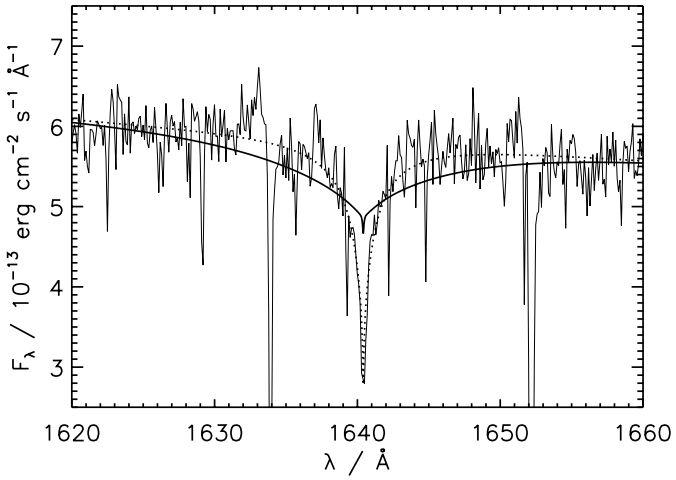

Fig. 9. He II line compared to a composite model (solid line) consisting of a DA spectrum of $T_{\rm eff} = 30\,000$ K with 85 % and a DO of $T_{\rm eff} = 50\,000$ K with 15 %. A DB model (dotted line) of $T_{\rm eff} = 36\,000$ K is also shown for comparison

50 000 K, but in the latter case, the He II 1640 Å line is broader than observed.

Fig. 9 illustrates this behaviour: A composite model consisting of a DA spectrum of $T_{\rm eff} = 30\,000$ K originating from 85 % of the surface and a DO of $T_{\rm eff} = 50\,000$ K covering 15 % has a He II line which is too broad and too shallow although the model can reproduce the strengths of both the Balmer and 4471 Å lines. For comparison, a DB model with $T_{\rm eff} = 35\,500$ K, which can reproduce the He II line, is also plotted.

The only remaining possibility to explain the spectrum of HS 0209+0832 with a static inhomogeneous surface composition would be a less extreme abundance variation – something like $\mathrm{He/H} = 0.5 \cdot 10^{-2}$ on one half of the star and $\mathrm{He/H} = 1.1 \cdot 10^{-2}$ on the other.

DA+DB double star. Jordan et al. (1993) have considered the possibility that HS 0209+0832 is a double star consisting of a DA and a DB white dwarf. This explanation has been sucessfully applied for the DABs MCT 0128−3846 and MCT 0453−2933 (Wesemael et al. 1994). Jordan et al. have found that a combination of a DA at $T_{\rm eff} = 32\,000$ K with a DB at 15 000 K can reproduce $\mathrm{H}\gamma$ and He I 4471 Å. However, the slope of the IUE spectrum indicated a higher temperature of the DA. The detection of the He II line at 4686 Å by Heber et al. (1997) and our finding of 1640 Å clearly rules out a cool DB as companion. The combination with a hotter DO would have the same problems as a helium spot model. Therefore, the spectrum cannot be explained with a DA+DB/DO binary.

5. Possible scenarios for HS 0209+0832

A successful model for HS 0209+0832 has to explain the (almost) homogeneous hydrogen-helium atmosphere, the presence of elements heavier than helium, and the variability at least of the helium features. In the following we discuss possible scenarios.

Accretion from the interstellar medium. Helium in atmospheres of DA white dwarfs is subject to downward diffusion on time scales much shorter than the cooling age so that the observed helium abundance in HS 0209+0832 cannot be of primordial origin. Radiation pressure is not strong enough to prevent helium from sinking: For $T_{\rm eff} = 35\,000$ K the expected abundance of helium is less than 10^{-7} (Vennes et al. 1988). It could be assumed that helium has indeed left the outer parts of the atmosphere so that a small hydrogen layer floats on top of the helium, but the analysis with stratified hydrogen-helium models in diffusion equilibrium shows that this scenario cannot reproduce the observations.

A rather homogeneous distribution of helium as it is implied by our analysis could be reached if helium has been accreted very recently from the interstellar medium onto the white dwarf. This scenario can also explain the observed variability of the helium abundance, if HS 0209+0832 has passed through regions with different densities and therefore experienced different accretion rates during the last years. A lower rate would reduce the abundance within a few months due to the short diffusion time scale. If we assume that the primordial helium has settled down then the outer hydrogen layer must have a mass of at least $M_{\rm H} \approx 10^{-15}\,M_{\odot}$. Otherwise, the underlying helium would disturb the observed spectral features. Koester (1989) has shown that hydrogen and helium are separated within nine months in a layer of this mass in a white dwarf with $T_{\rm eff} = 35\,000$ K; this is consistent with the possibility of a helium line strength variation within eight months as found by Heber et al. (1997).

The presence of heavy elements supports the assumption of recent accretion. In white dwarfs with $T_{\rm eff} \gtrsim 50\,000$ K metals can be supported against gravity by selective radiation pressure. However, this explanation is not possible for HS 0209+0832. Chayer et al. (1995) predict $\mathrm{C/H} = 6 \cdot 10^{-8}$, $\mathrm{Si/H} = 1 \cdot 10^{-7}$, and $\mathrm{Ca/H} = 3 \cdot 10^{-10}$. No recent calculations exist for titanium, nickel, and zinc but the nickel abundance should be similar to the iron abundance (Chayer et al. 1994), which is predicted to be less than 10^{-10}. The theoretical abundances are lower than the observed values for carbon, calcium, and nickel but higher for silicon. This implies that radiative levitation cannot account for the element abundances.

It is interesting to note that the atmosphere of HS 0209+0832 contains among others those metals (Ca, Ti, Al, Ni) which show the highest depletion factors of up to 1000 in the gas phase of the interstellar medium (e.g. in ζ Oph, Savage & Sembach 1996). This is commonly explained by their high condensation temperatures (cf. Spitzer 1978, Fig. 9.1). The large depletion of elements like calcium and titanium is a result of initial grain condensation in a dense and warm gas, e.g. in the winds of cool giants, where all calcium and titanium is condensed. Later, in a cooler medium, elements with lower accretion temperatures are accreted onto the condensation nuclei. It might be speculated that during infall from the interstellar medium the former con-

densation nuclei mostly survive the accretion process and reach the white dwarf surface while metals with lower condensation temperatures evaporate earlier and do not reach the atmosphere. However, the presence of zinc with a much lower condensation temperature does not fit into this scenario.

Accretion from a late-type companion. An alternative to accretion from the interstellar medium is accretion of helium and metals from a close companion. This scenario is discussed for some DAO white dwarfs at $T_{\rm eff} \gtrsim 50\,000$ K (e.g. Tweedy et al. 1993, Dobbie et al. 1999, Vennes et al. 1999). These objects and HS 0209+0832 have several similarities: Helium is distributed homogeneously in the atmosphere, an equilibrium stratified composition can be ruled out from the shape of the He II 1640 Å line (Vennes et al. 1999), the helium abundance of one object (EUVE J0720−317) seems to vary by one order of magnitude on a time scale of a year (Finley et al. 1997) or may be distributed inhomogeneously over the surface (Dobbie et al. 1999), and photospheric carbon is also detected (Thorstensen et al. 1996, Vennes et al. 1999). The main differences besides the temperature are that the helium abundance in HS 0209+0832 is about one order of magnitude higher and that the optical spectrum does not show any signs of emission lines from the companion whereas these lines are clearly detected in these DAO stars.

We have tested if a close, possibly interacting, M dwarf could be detected in the optical spectra of HS 0209+0832. The observed flux at 5500 Å and the theoretical visual magnitude according to the evolutionary tracks of Wood (1994, "thick" hydrogen layers) give a distance modulus of $m_{\rm V} - M_{\rm V} = 4.6$ for HS 0209+0832. The spectra of an M1V and an M5V star taken from the compilation of Jacoby et al. (1984) were scaled according to the distance modulus and the calibrated absolute magnitudes for these stars (Schmidt-Kaler 1982). The M dwarf spectra were than added to the synthetic DAB spectrum for HS 0209+0832 which was also scaled to the visual magnitude. The result is that even an M5V star would cause detectable absorption bands around 6200 Å. If there is indeed a companion star then the spectral type must be later than M5.

Magnetic fields. In the case of Feige 7 it has been discussed that a magnetic field between about 17 MG and 57 MG is the reason for the inhomogeneous surface composition (Achilleos et al. 1992): In regions of higher field strengths convection may be suppressed so that the outer hydrogen layer is not mixed fully with the underlying helium. However, this scenario can be ruled out here because the photosphere of HS 0209+0832 is convectively stable.

From the observed line shapes of the hydrogen lines we derive a maximum line splitting of $\pm$ 10 Å for Hβ and Hγ and $\pm$ 1.5 Å for Lα. This translates into an upper limit of 0.5 MG for the magnetic field strength. A sharper limit of $\approx$ 0.1 MG can be calculated from the C IV and Si IV lines and a maximum splitting of 0.05 Å due to anomalous Zeeman effect. Therefore, we believe that magnetic fields are not important in HS 0209+0832.

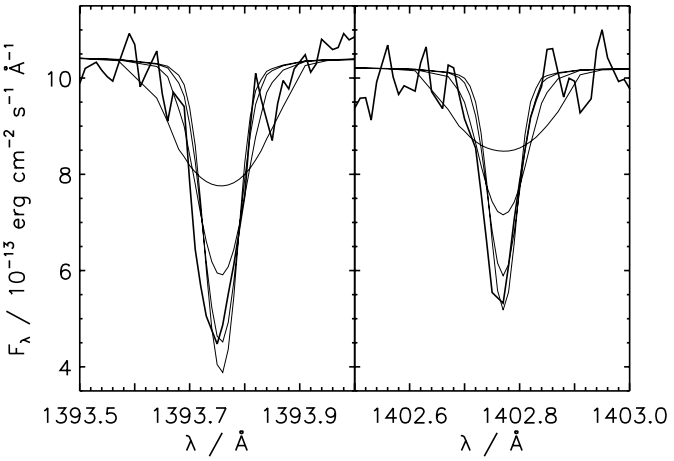

Fig. 10. Observed Si IV lines compared to rotational broadened models. From top to bottom: $v \sin i = 25$, 12.5, 6, 0 km s^{-1}

Rotation and meridional circulation. A mechanism that could explain a rather homogeneous distribution of helium would be large-scale meridional circulation in a rotating star. For a 0.8 $M_\odot$ white dwarf with $L = 10^{-2}\,L_\odot$ and a rotation velocity of 50 km s^{-1} Tassoul & Tassoul (1983) have found that mixing due to meridional circulation is completely negligible. The effect may be significantly stronger in HS 0209+0832 with $M \approx 0.6\,M_\odot$ and $L \approx 3 \cdot 10^{-1}\,L_\odot$. However, from the metal lines we derive an upper limit of 6 km s^{-1} for $v \sin i$ so that rotation should be not important unless the star is seen pole-on. Fig. 10 presents an example for the broadening due to rotation.

6. Discussion

We have investigated four models to explain the photospheric features of HS 0209+0832: a homogeneously mixed hydrogen-helium atmosphere, a stratified atmosphere in diffusion equilibrium, a helium abundance varying over the stellar surface, and a DA+DB double star. A stratified model with hydrogen and helium in diffusion equilibrium and a double star with extreme differences of chemical compositions can be clearly ruled out. Abundance variations over the stellar surface like single spots of pure helium surrounded by hydrogen are also not successful. The simplest model gives the best results: All spectral features can be reproduced very well with a homogeneous atmosphere.

Since the time scales for downward diffusion of helium are much shorter than the cooling times there must be a process which can compensate for the gravitational settling of helium. Such mechanisms can be ongoing accretion, meridional circulation, or surface inhomogeneties possibly caused by magnetic fields. As shown in Sect. 3 the latter two possibilities are rather unlikely so that we consider ongoing accretion as the most probable reason for the unusual photospheric composition of HS 0209+0832. This scenario has the advantage that it can explain both the helium content and the presence of heavier elements. Our analysis shows also that the abundances for He II, C IV, and Ti IV are higher than the abundances for He I, C III, and Ti III, respectively. This is probably either a non-LTE ef-

fect or an indication that significant amounts of these elements have already been diffused into deeper and hotter layers (see Sect. 3.2). However, diffusion equilibrium has not been reached due to ongoing accretion.

Accretion can occur from the interstellar/circumstellar environment or from mass exchange with a companion star. Since there are no indications for a companion and since only two velocity systems (ISM and photospheric) could be detected in the UV spectrum, the interstellar accretion scenario seems to be most probable – although we cannot fully exclude that some of the unidentified lines originate in an interstellar/circumstellar environment with a different velocity. It is possible that the interstellar lines detected in our HST spectrum originate in the cloud surrounding the white dwarf.

The variation of the helium abundance as observed by Heber et al. (1997) can be explained, if HS 0209+0832 currently crosses a region of the interstellar medium with an inhomogeneous density. The time scale for separation of hydrogen and helium is about nine months (Koester 1989) so that a lower accretion rate results immediately in a reduced helium abundance. This can explain the different measurements of helium in observations separated by about eight months. Since the variability measurement rests on only one observation and could not be repeated it cannot, however, be fully excluded that the helium abundance is actually constant. The only hint for a variable metal abundance is the different strength of C IV 1548 Å in the IUE and HST spectra, but the reality of this measurement is doubtful due to the low S/N ratio of the IUE spectrum.

The accretion rate necessary to explain our observations can be estimated, since the thickness of the visible hydrogen envelope is about $\approx 10^{-15}\,M_{\odot}$ (Sect. 5). In order to account for 1 % of helium (by numbers), $10^{-16}\ M_{\odot}$ of matter with solar helium abundance must be accreted on a time scale of about nine months. This value is similar to the accretion rate during an encounter with an interstellar cloud assumed by Dupuis et al. (1993) to explain the presence of metals in cool DZ white dwarfs.

How does HS 0209+0832 fit into the scenario for the evolution of the spectral sequence? The prototype DAB star GD 323 is not compatible with a homogeneously mixed hydrogen-helium atmosphere (Liebert et al. 1984, Koester et al. 1994) whereas the hotter DAOs can be explained better with homogeneous than with stratified atmospheres (Bergeron et al. 1994). Mass loss may play an important role for delaying diffusion equilibrium between hydrogen and helium in DAOs (Unglaub & Bues 1998), but at 35 000 K this can be excluded for HS 0209+0832.

Considering the isolated place of this star inside the DB gap it seems probable that it is not related to other DABs/DAOs and that the important physical mechanisms are different from that of other DAB or DAO white dwarfs. If this is true HS 0209+0832 is not representative for a former DO star which is currently hiding as a DA (with traces of the former atmospherical helium content) before He II convective mixing at $T_{\rm eff} = 28\,000$ K will transform it into a helium-rich DB again. Since the helium is probably accreted only recently it is not possible to tell whether the star has a thick hydrogen envelope and therefore has been a DA during the whole cooling sequence or whether it has been a DO with a hydrogen mass just thick enough that the hydrogen layer is not transparent for the underlying helium.

For a test of our favored scenario it would be very useful to observe HS 0209+0832 on a time scale of a few months in order to monitor possible variations of the helium abundance due to an inhomogeneous interstellar medium or due to slow rotation. Additional UV observations would help to find out whether the metal content remains constant or is also changing with time.

Acknowledgements. This work has been supported by the Deutsches Zentrum für Luft- und Raumfahrt (DLR) under grant 50 OR 96173. DK thanks Dr. Jay Holberg and Dr. Jim Liebert for their hospitality during summer 2000 at the University of Arizona and the Deutsche Forschungsgemeinschaft (DFG) for a travel grant. We are grateful to the referee Dr. Stephane Vennes for his helpful comments and particularly for his identification of Zn III.

References

Achilleos N., Wickramasinghe D.T., Liebert J., Saffer R.A., Grauer A.D., 1992, ApJ 396, 273
Beauchamp A., Wesemael F., Fontaine G., Bergeron P., 1993, In: Barstow M. (ed.) White Dwarfs: Advances in Observations and Theory. Kluwer, Dordrecht, p. 281
Bergeron P., Wesemael F., Beauchamp A., et al., 1994, ApJ 432, 305
Bruhweiler F., Kondo Y., 1981, ApJ 248, L123
Chayer P., LeBlanc F., Fontaine G., et al., 1994, ApJ 436, L161
Chayer P., Vennes S., Pradhan A.K., et al., 1995, ApJ 454, 429
Crooker A.M., Dick K.A., 1968, Canad. J. Phys. 46, 1241
Dobbie P.D., Barstow M.A., Burleigh M.R., Hubeny I., 1999, A&A 346, 163
Dupree A.K., Raymond J.C., 1982, ApJ 263, L63
Dupuis J., Fontaine G., Pelletier C., Wesemael F., 1993, ApJS 84, 73
Fontaine G., Wesemael F., 1987, In: Philip A.G.D., Hayes D.S., Liebert J.W. (eds.) The Second Conference on Faint Blue Stars. IAU Coll. No. 95, L. Davis Press, Schenectady, p. 319
Finley D.S., Koester D., Basri G., 1997, ApJ 488, 375
Heber U., Napiwotzki R., Lemke M., Edelmann H., 1997, A&A 324, L53
Herwig F., Blöcker T., Langer N., Driebe T., 1999, A&A 349, L5
Holberg J.B., Kidder K.M., Wesemael F., 1990, ApJ 365, L77
Holberg J.B., Barstow M.A., Lanz T., Hubeny I., ApJ 484, 871
Iben Jr. I., McDonald J., 1995, In: Koester D., Werner K. (eds.) White Dwarfs. Springer, Berlin, p. 48
Jacoby G.H., Hunter D.A., Christian C.A., 1984, ApJS 56, 257
Jenkins E.B., Drake J.F., Morton D.C., 1973, ApJ 181, L122
Jordan S., Koester D., 1986, A&AS 65, 367
Jordan S., Heber U., Engels D., Koester D., 1993, A&A 273, L27
Kidder K.M., Holberg J.B., Barstow M.A., Tweedy R.W., Wesemael F., 1992, ApJ 394, 288
Koester D., 1989, In: Wegner G. (ed.) White Dwarfs. IAU Colloquium No. 114, Springer, Berlin, p. 206
Koester D., Liebert J., Saffer R.A., 1994, ApJ 422, 783
Kurucz R., Bell B., 1995, Kurucz CD-ROM No. 23, Smithsonian Astrophysical Observatory, Cambridge, Massachusetts
Liebert J., Wesemael F., Sion E.M., Wegner G., 1984, ApJ 277, 692
Liebert J., Wesemael F., Hansen C.J., et al., 1986 ApJ 309, 241
Meinders E., 1976, Physica 84C, 117
Savage B.D., Sembach K.R., 1996, ApJ 470,893

Schatzman E., 1949, Le Spectre des Naines blanches et leur Débit d'Énergie. Publikationer og mindre Meddelelser fra Københavns Observatorium Vol. 149, Copenhagen
Schatzman E., 1958, White Dwarfs. North-Holland Publishing Company, Amsterdam
Schmidt-Kaler, T., 1982. In: Schaefer K., Voigt H.H. (eds.) Landolt-Börnstein: Numerical Data and Functional Relationships in Science and Technology. Vol. VI/2b, Springer, Berlin, p. 451
Spitzer, L., 1978, Physical Processes in the Interstellar Medium. John Wiley & Sons, New York
Sugar J., Musgrove A., 1995, J. Phys. Chem. Ref. Data 24, 1803
Tassoul M., Tassoul J.-L., 1983, ApJ 267, 334
Thorstensen J.R., Vennes S., Bowyer S., 1996, ApJ 457, 390
Tweedy R.W., Holberg J.B., Barstow M.A., et al., 1993 AJ 105, 1938
Unglaub K., Bues I., 1998, A&A 338, 75
van Dishoek E.F., Black J.H., 1984, ApJS 62, 109
Vennes S., Pelletier C., Fontaine G., Wesemael F., 1988, ApJ 331, 876
Vennes S., Bowyer S., Dupuis J., 1996, ApJ 461, L103
Vennes S., Thorstensen J.R., Polomski E.F., 1999, ApJ 523, 386
Wesemael F., Bergeron P., Lamontagne R., et al., 1994, ApJ 429, 369
Wood M.A., 1994, In: Chabrier G., Schatzman E. (eds.) The Equation of State in Astrophysics. IAU Coll. 147, Cambridge University Press, p. 612